Supporting Information

for

Structural Details of Light Activation of the LOV2-based Photoswitch PA-Rac1

Andreas Winkler[†], Thomas R.M. Barends[†], Anikó Udvarhelyi[†], Daniel Lenherr-Frey[†], Lukas Lomb[†], Andreas Menzel[‡] and Ilme Schlichting[†,*]

[†] Department of Biomolecular Mechanisms, Max Planck Institute for Medical Research, Heidelberg, 69120, Germany

[‡] Coherent X-ray Scattering Group, Paul Scherrer Institute, Villigen, 5232, Switzerland

Correspondence should be addressed to I.S. (Ilme.Schlichting@mpimf-heidelberg.mpg.de)

SUPPLEMENTARY FIGURES

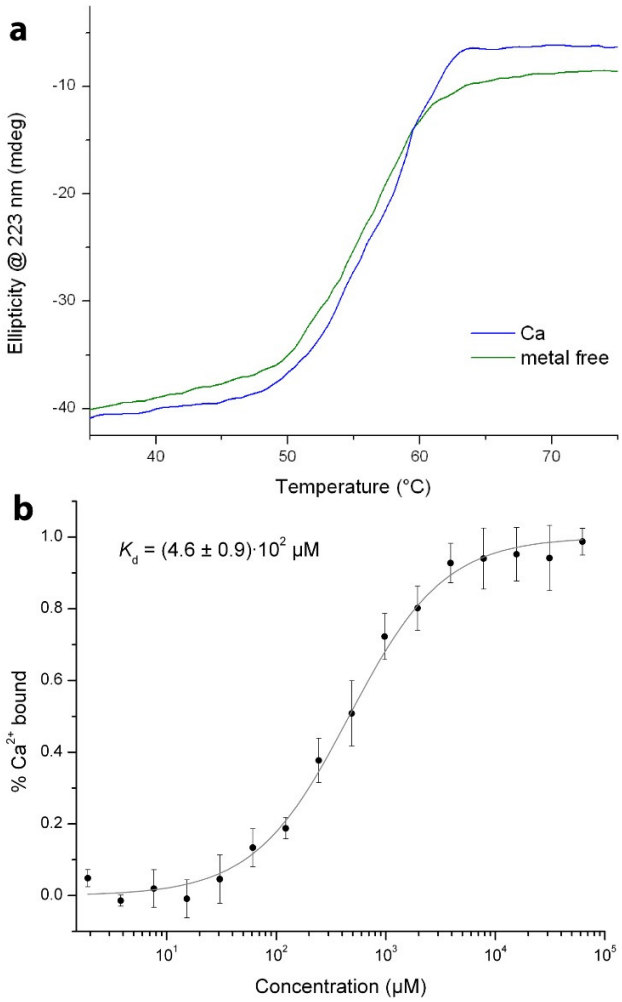

Supplementary Figure 1. Calcium binding to PA-Rac1. (a) Melting curves of PA-Rac1 followed by CD spectroscopy. The estimated T_m of metal free (green) and calcium bound (blue) samples is 55 °C and 57 °C, respectively. (b) Affinity of calcium binding to PA-Rac1 determined by microscale thermophoresis. Error bars correspond to the standard deviation from six measurements.

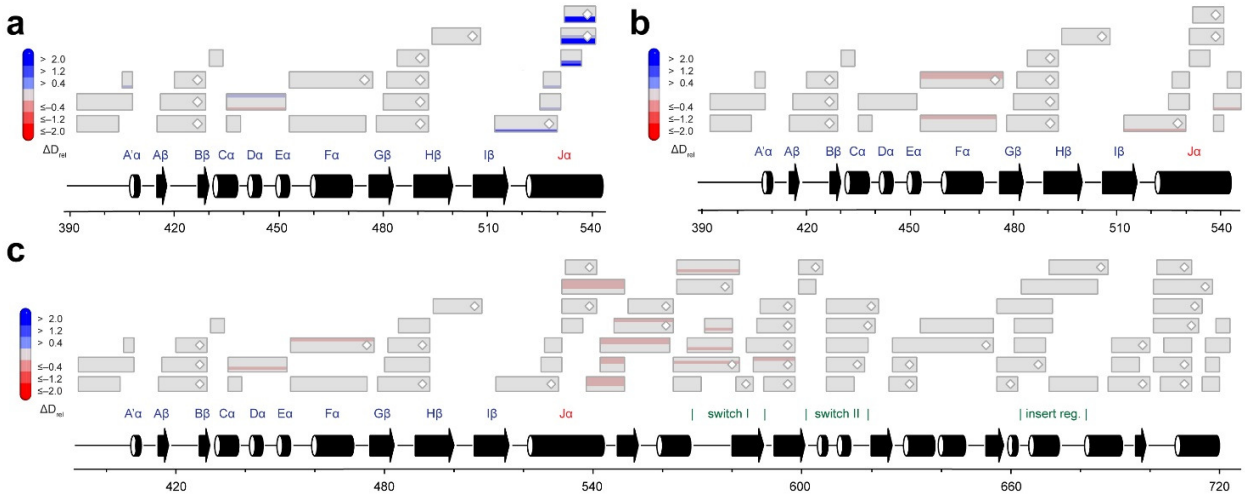

Supplementary Figure 2. Comparison of HDX characteristics of LOV2 peptides. Each box corresponds to one peptide and contains five different colors according to the legend for the incubation times of 10, 45, 180, 900 and 3600 s (bottom up). MS/MS confirmed peptides are marked with diamonds. Secondary structure elements are taken from DSSP (Define Secondary Structure of Proteins) analysis of PA-Rac1 (pdb 2wkp)[8]. (a) Effects on the LOV2-Rac1 interface in the presence of calcium (D_{rel} of $PA_{Ca,d}$ – D_{rel} of $LOV_{Ca,d}$) (b) Effect of calcium binding on isolated LOV2 (D_{rel} of $LOV_{Ca,d}$ – D_{rel} of $LOV_{mf,d}$). (c) Calcium influence on light activated PA-Rac1 (D_{rel} of $PA_{Ca,l}$ – D_{rel} of $PA_{mf,l}$).

Supplementary Figures 3–5. Overview of peptides evaluated during HDX analysis of LOV2 and PA-Rac1. Full page views of individual comparisons are provided with deuterium incorporation plots of all 25 and 73 peptides, respectively. Zoom in on the region of interest for full details. Supplementary Figures 3, 4 and 5 correspond to $LOV_{mf,d}$ (cyan) + $LOV_{Ca,d}$ (magenta), $PA_{mf,d}$ (green) + $PA_{mf,l}$ (orange) and $PA_{Ca,d}$ (blue) + $PA_{Ca,l}$ (red), respectively. Individual deuterium incorporation plots show the time dependent increase in relative deuterium levels in the main panel. D_{rel} values are shown as the mean of three independent measurements and error bars correspond to the standard deviation. A software-estimated abundance distribution of deuterated species is presented in the lower sub-panel on a scale from undeuterated to all exchangeable amides deuterated[23].

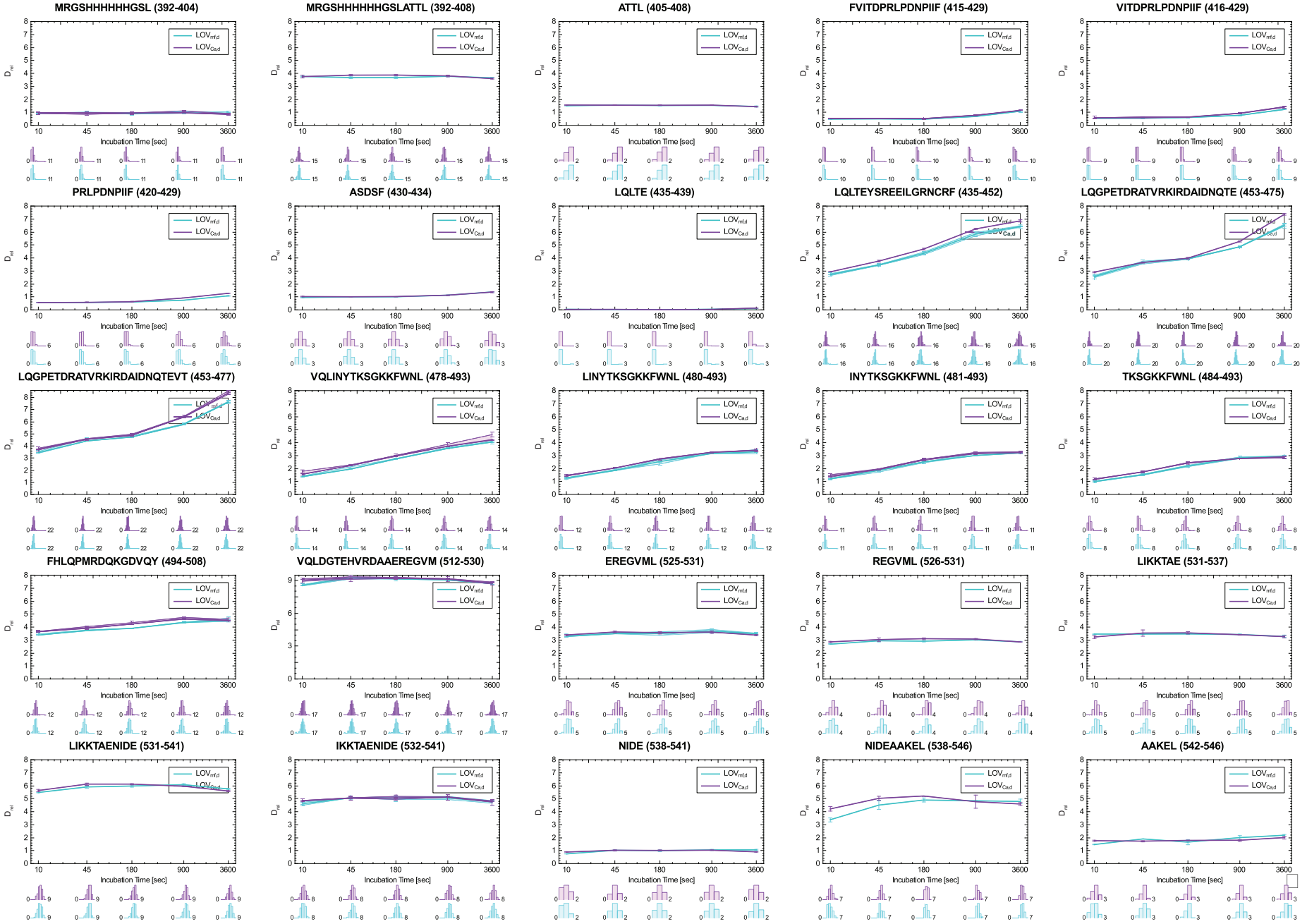
MRGSHHHHHHGSL (392-404)
MRGSHHHHHHGSLATTL (392-408)
ATTL (405-408)
FVITDPRLPDNPIIF (415-429)
VITDPRLPDNPIIF (416-429)
PRLPDNPIIF (420-429)
ASDSF (430-434)
LQLTE (435-439)
LQLTEYSREEILGRNCRF (435-452)
LQGPETDRATVRKIRDAIDNQTE (453-475)
LQGPETDRATVRKIRDAIDNQTEVT (453-477)
VQLINYTKSGKKFWNL (478-493)
LINYTKSGKKFWNL (480-493)
INYTKSGKKFWNL (481-493)
TKSGKKFWNL (484-493)
FHLQPMRDQKGDVQY (494-508)
VQLDGTEHVRDAAEREGVM (512-530)
EREGVML (525-531)
REGVML (526-531)
LIKKTAE (531-537)
LIKKTAENIDE (531-541)
IKKTAENIDE (532-541)
NIDE (538-541)
NIDEAAKEL (538-546)
AAKEL (542-546)
Incubation Time [sec]
10
45
180
900
3600
D_rel
LOV_mf,d
LOV_Ca,d

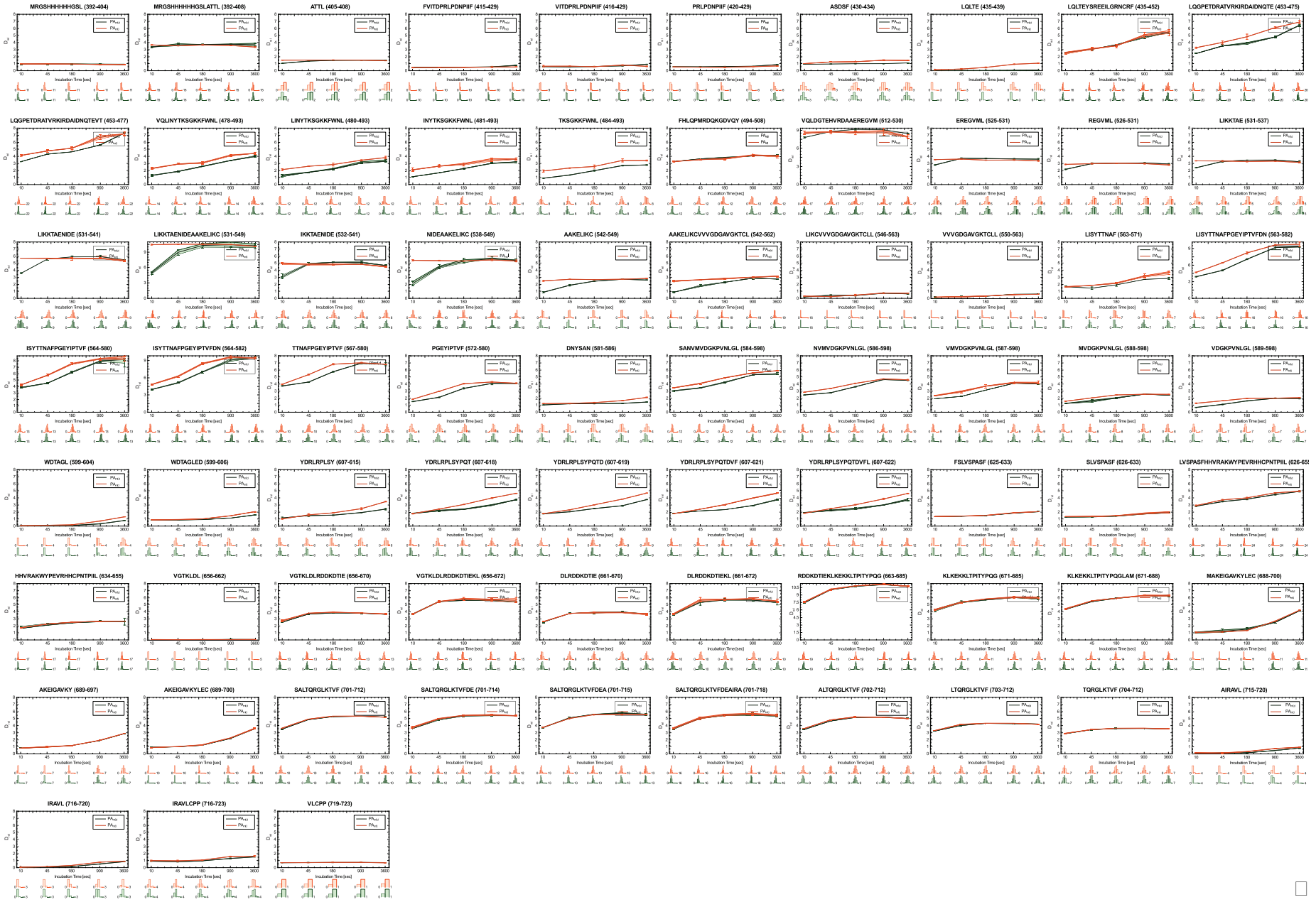
MRGSHHHHHHGSL (392-404)
MRGSHHHHHHGSLATTL (392-408)
ATTL (405-408)
FVITDPRLPDNPIIF (415-429)
VITDPRLPDNPIIF (416-429)
PRLPDNPIIF (420-429)
ASDSF (430-434)
LQLTE (435-439)
LQLTEYSREEILGRNCRF (435-452)
LQGPETDRATVRKIRDAIDNQTE (453-475)
LQGPETDRATVRKIRDAIDNQTEVT (453-477)
VQLINYTKSGKKFWNL (478-493)
LINYTKSGKKFWNL (480-493)
INYTKSGKKFWNL (481-493)
TKSGKKFWNL (484-493)
FHLQPMRDQKGDVQY (494-508)
VQLDGTEHVRDAAEREGVM (512-530)
EREGVML (525-531)
REGVML (526-531)
LIKKTAE (531-537)
LIKKTAENIDE (531-541)
LIKKTAENIDEAAKELIKC (531-549)
IKKTAENIDE (532-541)
NIDEAAKELIKC (538-549)
AAKELIKC (542-549)
AAKELIKCVVVGDGAVGKTCL (542-562)
LIKCVVVGDGAVGKTCLL (546-563)
VVVGDGAVGKTCLL (550-563)
LISYTTNAF (563-571)
LISYTTNAFPGEYIPTVFDN (563-582)
ISYTTNAFPGEYIPTVF (564-580)
ISYTTNAFPGEYIPTVFDN (564-582)
TTNAFPGEYIPTVF (567-580)
PGEYIPTVF (572-580)
DNYSAN (581-586)
SANVMVDGKPVNLGL (584-598)
NVMVDGKPVNLGL (586-598)
VMVDGKPVNLGL (587-598)
MVDGKPVNLGL (588-598)
VDGKPVNLGL (589-598)
WDTAGL (599-604)
WDTAGLED (599-606)
YDRLRPLSY (607-615)
YDRLRPLSYPQT (607-618)
YDRLRPLSYPQTD (607-619)
YDRLRPLSYPQTDVF (607-621)
YDRLRPLSYPQTDVFL (607-622)
FSLVSPASF (625-633)
SLVSPASF (626-633)
LVSPASFHHVRAKWYPEVRHHCPNTPIIL (626-65
HHVRAKWYPEVRHHCPNTPIIL (634-655)
VGTKLDL (656-662)
VGTKLDLRDDKDTIE (656-670)
VGTKLDLRDDKDTIEKL (656-672)
DLRDDKDTIE (661-670)
DLRDDKDTIEKL (661-672)
RDDKDTIEKLKEKKLTPITYPQG (663-685)
KLKEKKLTPITYPQG (671-685)
KLKEKKLTPITYPQGLAM (671-688)
MAKEIGAVKYLEC (688-700)
AKEIGAVKY (689-697)
AKEIGAVKYLEC (689-700)
SALTQRGLKTVF (701-712)
SALTQRGLKTVFDE (701-714)
SALTQRGLKTVFDEA (701-715)
SALTQRGLKTVFDEAIRA (701-718)
ALTQRGLKTVF (702-712)
LTQRGLKTVF (703-712)
TQRGLKTVF (704-712)
AIRAVL (715-720)
IRAVL (716-720)
IRAVLCPP (716-723)
VLCPP (719-723)
Incubation Time [sec]
10
45
180
900
3600


MRGSHHHHHHGSL (392-404)
MRGSHHHHHHGSLATTL (392-408)
ATTL (405-408)
FVITDPRLPDNPIIF (415-429)
VITDPRLPDNPIIF (416-429)
PRLPDNPIIF (420-429)
ASDSF (430-434)
LQLTE (435-439)
LQLTEYSREEILGRNCRF (435-452)
LGQPETDRATVRKIRDAIDNQTEVT (453-477)
VQLINYTKSGKKFWNL (478-493)
LINYTKSGKKFWNL (480-493)
INYTKSGKKFWNL (481-493)
TKSGKKFWNL (484-493)
FHLQPMRDQKGDVQY (494-508)
VQLDGTEHVRDAAEREGVM (512-530)
EREGVML (525-531)
REGVML (526-531)
LIKKTAE (531-537)
LIKKTAENIDE (531-541)
LIKKTAENIDEAAKELIKC (531-549)
IKKTAENIDE (532-541)
NIDEAAKELIKC (538-549)
AAKELIKC (542-549)
AAKELIKCVVVGDGAVGKTCL (542-562)
LIKCVVVGDGAVGKTCLL (546-563)
VVVGDGAVGKTCLL (550-563)
LISYTTNAF (563-571)
LISYTTNAFPGEYIPTVFDN (563-582)
ISYTTNAFPGEYIPTVF (564-580)
ISYTTNAFPGEYIPTVFDN (564-582)
TTNAFPGEYIPTVF (567-580)
PGEYIPTVF (572-580)
DNYSAN (581-586)
SANVMVDGKPVNLGL (584-598)
NVMVDGKPVNLGL (586-598)
VMVDGKPVNLGL (587-598)
MVDGKPVNLGL (588-598)
VDGKPVNLGL (589-598)
WDTAGL (599-604)
WDTAGLED (599-606)
YDRLRPLSY (607-615)
YDRLRPLSYPQT (607-618)
YDRLRPLSYPQTD (607-619)
YDRLRPLSYPQTDVF (607-621)
YDRLRPLSYPQTDVFL (607-622)
FSLVSPASF (625-633)
SLVSPASF (626-633)
LVSPASFHHVRAKWYPEVRHHCPNTPIIL (626-65
HHVRAKWYPEVRHHCPNTPIIL (634-655)
VGTKLDL (656-662)
VGTKLDLRDDKDTIE (656-670)
VGTKLDLRDDKDTIEKL (656-672)
DLRDDKDTIE (661-670)
DLRDDKDTIEKL (661-672)
RDDKDTIEKLKEKKLTPITYPQG (663-685)
KLKEKKLTPITYPQG (671-685)
KLKEKKLTPITYPQGLAM (671-688)
MAKEIGAVKYLEC (688-700)
AKEIGAVKY (689-697)
AKEIGAVKYLEC (689-700)
SALTQRGLKTVF (701-712)
SALTQRGLKTVFDE (701-714)
SALTQRGLKTVFDEA (701-715)
SALTQRGLKTVFDEAIRA (701-718)
ALTQRGLKTVF (702-712)
LTQRGLKTVF (703-712)
TQRGLKTVF (704-712)
AIRAVL (715-720)
IRAVL (716-720)
IRAVLCPP (716-723)
VLCPP (719-723)
Incubation Time [sec]

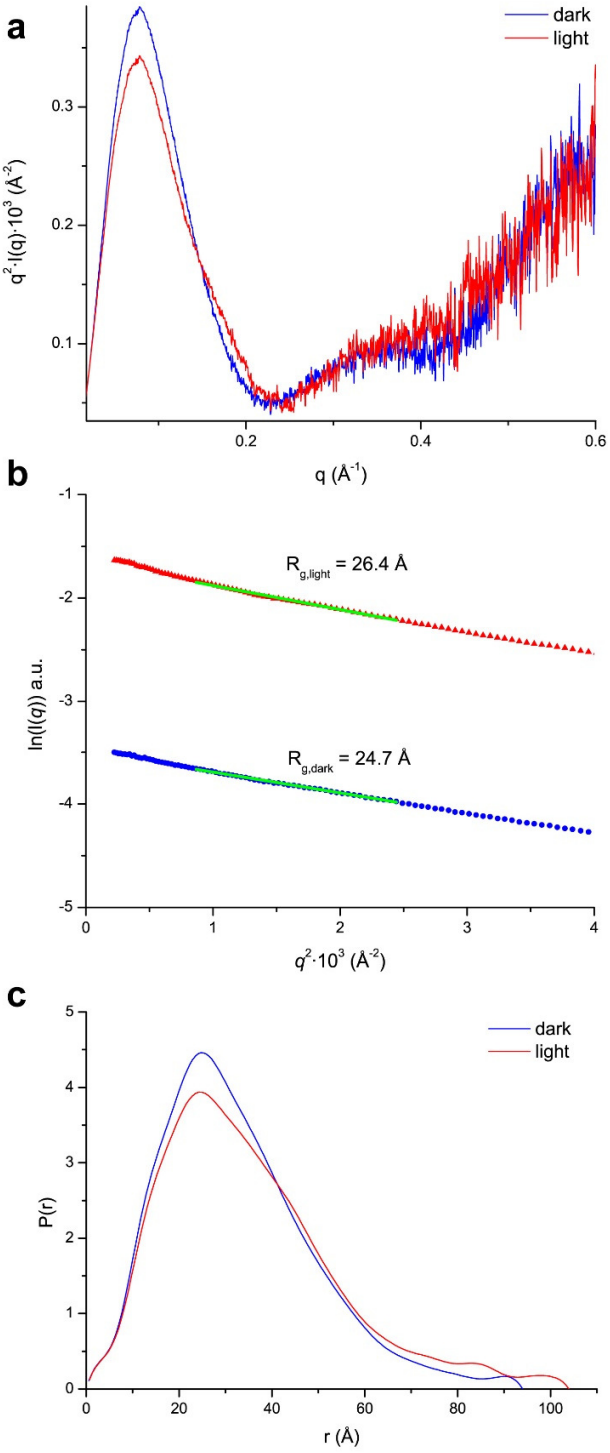

Supplementary Figure 6. SAXS data of dark and light state PA-Rac1. (a) Kratky plots of averaged dark-state data (blue) and light-state data (red). The latter were extracted from SVD analysis of time-resolved solution scattering experiments. (b) Guinier plots of dark- and light-state SAXS data, showing a slightly increased R_g for the light state data. The light state data are shifted vertically for better visualization. Both liner fits (green) fulfill the criteria of $q_{max} \cdot Rg \leq 1.3$. (c) Pair distance distribution functions of dark and light-state data of PA-Rac1 calculated using GNOM[48].

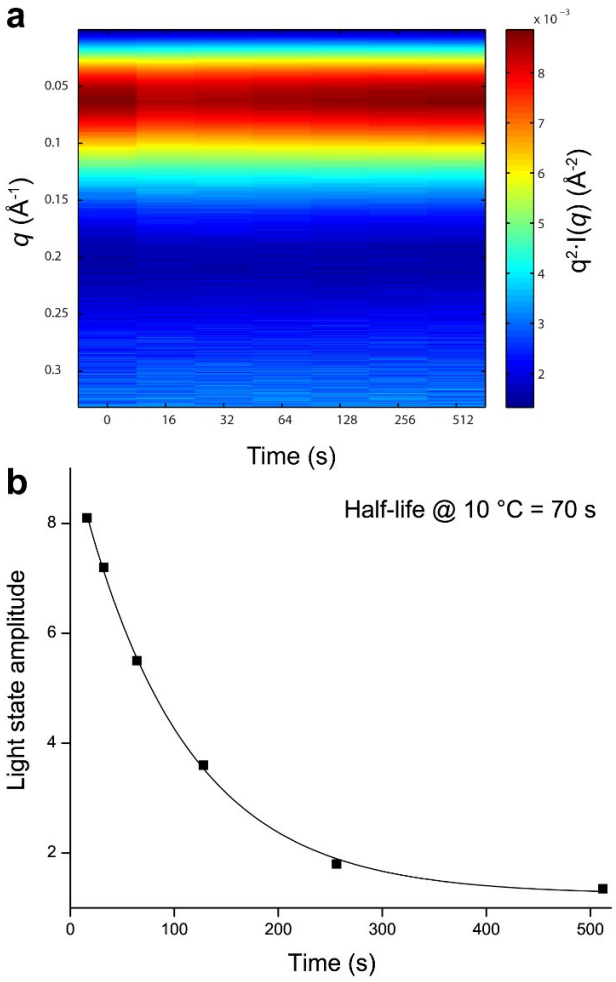

Supplementary Figure 7. Control experiments for the PA-Rac1 solution scattering studies. (a) The reversibility of the characteristic light-induced changes during the dark state recovery is visualized by heat map representations of Kratky plots (cf. Supplementary Fig. 6a) calculated from the scattering curves at the various time points. (b) Dark-state recovery kinetics of PA-Rac1 after an initial 500 ms blue-light illumination pulse. The reported light state amplitude corresponds to the contribution of the PA-Rac1 light state scattering signal obtained by SVD analysis. A single exponential decay function was used to fit the data and, considering the temperature dependence of rate constants, the extracted half-life of 70 s at 10 °C nicely corresponds to the 43 s obtained for PA-Rac1 at room temperature[8].

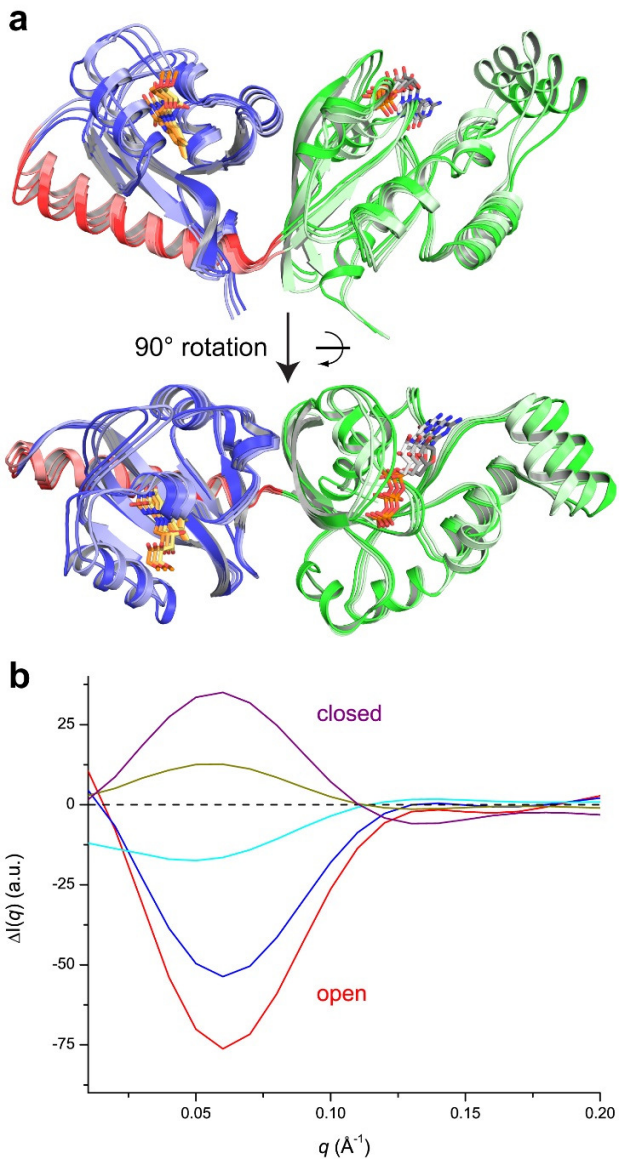

Supplementary Figure 8. NMA of PA-Rac1. (a) Three individual substructures of the clam-shell opening mode obtained for pdb 2wkp[8]. The substructures are colored according to Figure 1a with darkened colors along the opening movement. Metal ions are omitted for clarity. (b) Difference spectra of calculated radial density distributions of individual substructures from the PA-Rac1 normal mode shown in panel a versus the calculated scattering curve of the dark-state crystal structure (pdb 2wkp)[8]. The red line corresponds to the open conformation and additional spectra correspond to the clam-shell closing mode passing the crystal structure (dashed black line) towards a closed state (purple spectrum). The axis settings are analogous to Figure 5d for easier comparison.

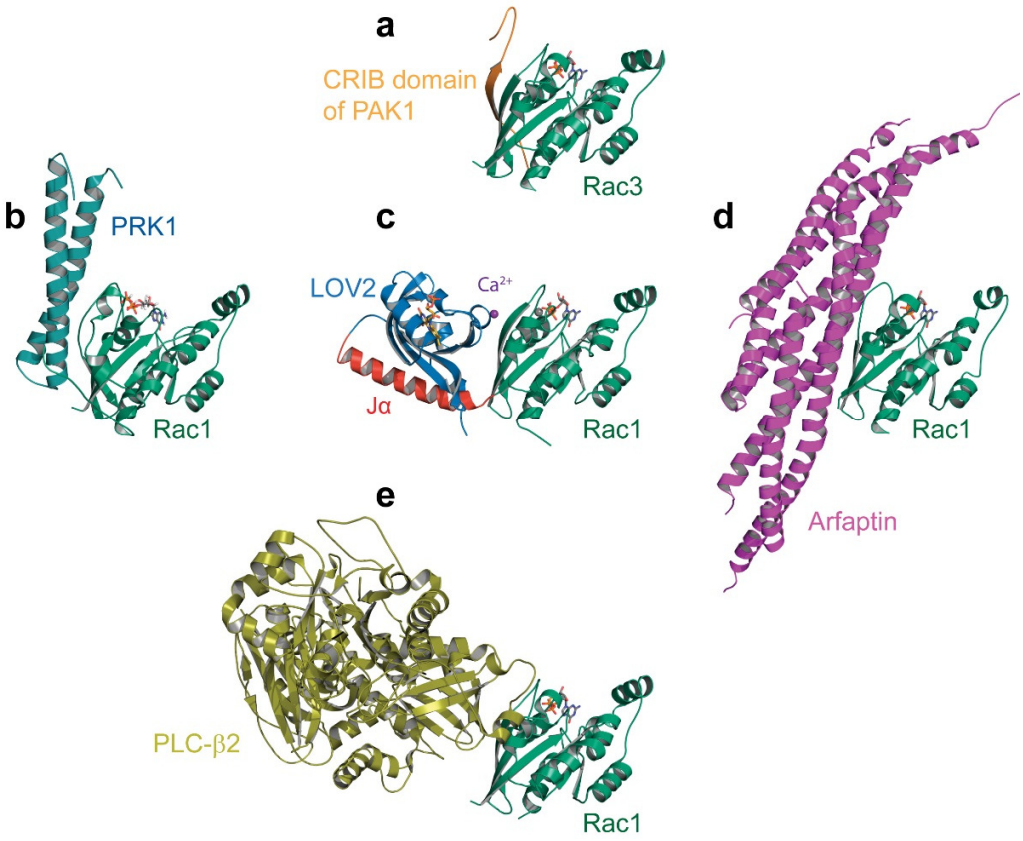

Supplementary Figure 9. Comparison of Rac-GTPase interactions with different effectors. All structures are aligned based on the GTPase domain and shown in the same orientation as PA-Rac1 in Figure 1a. For easier comparison PA-Rac1 is also included in the central panel c, to illustrate the overlap of the calcium binding site with all effector interaction regions. (a) Structure of human Rac3 with the CRIB domain of PAK1 (pdb 2qme, Structural Genomics Consortium). (b) The complex of human Rac1 with protein kinase C-related kinase 1 (PRK1, pdb 2rmk)[51]. (c) PA-Rac1 (pdb 2wkp)[8]. (d) Crystal structure of human Rac1 with arfaptin (pdb 1i4t)[52]. (e) Rac1 bound to its effector phospholipase C beta 2 (PLC-β2, pdb 2fju)[53].

WEB-ENHANCED OBJECTS – SUPPLEMENTARY MOVIES

Supplementary Movie 1. Animation of time-dependent changes in deuterium incorporation upon calcium binding in the dark. The time series of $PA_{Ca,d}$ – $PA_{mf,d}$ comparisons is presented with colors corresponding to the differences in D_{rel} according to the bar-legend. Red or blue colors reflect an increased or decreased deuterium uptake, respectively, upon calcium-coordination. FMN and GTP are shown as orange and gray stick models, respectively, and the calcium and magnesium ions as purple and gray spheres. The animation is related to Figure 4a.

Supplementary Movie 2. Animation of time-dependent changes in deuterium incorporation upon blue-light illumination in the presence of calcium. The time series of $PA_{Ca,l}$ – $PA_{Ca,d}$ comparisons is presented with colors corresponding to the differences in D_{rel} according to the bar-legend. Red or blue colors reflect an increased or decreased deuterium uptake, respectively, upon illumination in the presence of Ca^{2+}. FMN and GTP are shown as orange and gray stick models, respectively, and the calcium and magnesium ions as purple and gray spheres. The animation is related to Figure 4b.

SUPPLEMENTARY REFERENCES

1.–50. Supplementary Information references 1–50 follow main text numbering.

51. Modha, R., Campbell, L. J., Nietlispach, D., Buhecha, H. R., Owen, D., and Mott, H. R. (2008) The Rac1 polybasic region is required for interaction with its effector PRK1, *J. Biol. Chem. 283*, 1492-1500.

52. Tarricone, C., Xiao, B., Justin, N., Walker, P. A., Rittinger, K., Gamblin, S. J., and Smerdon, S. J. (2001) The structural basis of Arfaptin-mediated cross-talk between Rac and Arf signalling pathways, *Nature 411*, 215-219.

53. Jezyk, M. R., Snyder, J. T., Gershberg, S., Worthylake, D. K., Harden, T. K., and Sondek, J. (2006) Crystal structure of Rac1 bound to its effector phospholipase C-beta2, *Nat. Struct. Mol. Biol. 13*, 1135-1140.